



## TiO<sub>2</sub>/BiVO<sub>4</sub> composite from preformed nanoparticles for heterogeneous photocatalysis

Fernando C. Soares<sup>a,b,1</sup>, Jéssica C. de Almeida<sup>a,1</sup>, Rafaella H. Koga<sup>b</sup>,  
Douglas M. da Silva Del Duque<sup>b</sup>, Gelson T.S.T. da Silva<sup>c</sup>, Caue Ribeiro<sup>c</sup>, Vagner R. de  
Mendonça<sup>a,b,\*</sup>

<sup>a</sup> Graduate Program in Materials Science (PPGCM), Federal University of São Carlos - Campus Sorocaba, Rod. SP-264, km 110, Sorocaba, SP, CEP 18052-780, Brazil

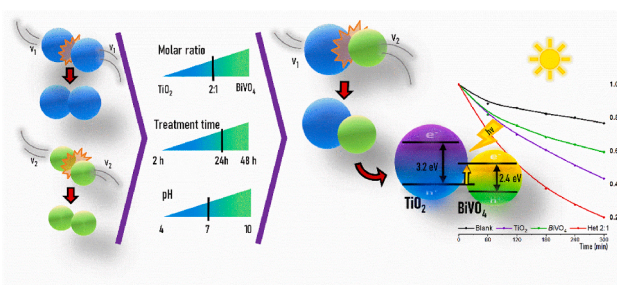
<sup>b</sup> Federal Institute of Science, Education, and Technology of São Paulo – Campus Itapetininga, Av. João Olímpio de Oliveira, 1561, Itapetininga, SP, CEP: 18208-000, Brazil

<sup>c</sup> Nanotechnology National Laboratory for Agriculture (LNNA), Embrapa Instrumentation, Rua XV de Novembro, 1452, CEP 13561-260, São Carlos, SP, Brazil

### HIGHLIGHTS

- TiO<sub>2</sub>/BiVO<sub>4</sub> heterostructures were obtained by heteroaggregation under hydrothermal conditions.
- Heterostructures were more efficient for Methylene Blue dye photodegradation than the isolated pristine materials.
- Materials performance could be tuned by controlling hydrothermal parameters.
- Heterostructures were active to photo-degrade the dye under solar light.
- Heterostructures were stable after six cycles and 67 days.

### GRAPHICAL ABSTRACT



### ARTICLE INFO

#### Keywords:

Composite  
Titanium dioxide  
Bismuth vanadate  
Interface  
Photodegradation

### ABSTRACT

Heteroaggregation of preformed nanocrystals used as building blocks is an interesting approach for the synthesis of heterostructures since it is possible to retain the main surface characteristics of the materials. In this paper, we studied the synthesis of a heterostructure consisting of monoclinic BiVO<sub>4</sub> and anatase TiO<sub>2</sub> phase for photocatalytic application. The heterostructures were synthesized using the building blocks technique with different TiO<sub>2</sub>/BiVO<sub>4</sub> molar ratios under hydrothermal treatment. The effectiveness of heteroaggregations formation results in more photoactive catalysts due to the possibility of electron transfer between the materials. Methylene Blue (MB) solutions were decolorized under ultraviolet and visible radiation to evaluate the samples' photocatalytic activity. As a result, the as-synthesized samples presented higher photocatalytic efficiency than pristine anatase TiO<sub>2</sub> and *m*-BiVO<sub>4</sub> precursors. The increase of the photocatalytic properties is mainly attributed to the separation of the photogenerated charges, which is the central feature of heterostructures formed due to the collision of the particles during hydrothermal treatment.

\* Corresponding author. Graduate Program in Materials Science (PPGCM), Federal University of São Carlos - Campus Sorocaba, Rod. SP-264, km 110, Sorocaba, SP, CEP 18052-780, Brazil.

E-mail address: [vrm@ifsp.edu.br](mailto:vrm@ifsp.edu.br) (V.R. de Mendonça).

<sup>1</sup> These authors contributed equally to this work.

<https://doi.org/10.1016/j.matchemphys.2022.126588>

Received 23 February 2022; Received in revised form 20 July 2022; Accepted 23 July 2022

Available online 17 August 2022

0254-0584/© 2022 Elsevier B.V. All rights reserved.

## 1. Introduction

In the past few decades, intensive research has been devoted to the heterogeneous photocatalysis process because of its promising potential for environmental pollution remediation applications [1–5]. In this process, semiconductors are exposed to light irradiation, inducing the formation of photogenerated electron-hole pairs capable of directly or indirectly degrading contaminant species [6–8].

The anatase TiO<sub>2</sub> is the pioneer of the semiconductor employed in the photocatalysis process. It is highlighted due to its high physical and chemical stability, low cost, and nontoxicity characteristics [4,9–11]. However, its large bandgap value of 3.2 eV is considered a limitation for large-scale applications using sunlight [11,12]. Conversely, the monoclinic BiVO<sub>4</sub> has the desired visible-light-responsive bandgap of 2.4 eV but with a fast electron-hole pairs recombination rate and poor photocatalytic activity [13,14].

An interesting approach for improving the properties of a catalyst is creating heterostructures composed of multiple semiconductors [15–20]. When an interface is created between two semiconductor surfaces with divergent bandgap values, the photogenerated charges can migrate to the conduction and valence bands of neighboring semiconductor particles. This electron-hole pair dispersion increases their lifespan, and, consequently, the photocatalytic efficiency is improved [6,21,22].

Although the formation of heterostructures is a feasible patch, the selection of the materials and methodology must be thorough to effectively induce the movement of the photogenerated charges in the interfacial region to the next semiconductor bands [23]. In this scope, the building blocks technique was proposed to assemble the heterostructures through particle coalescence [6,24,25]. This mechanism is usual in forming anisotropic crystals and is an interesting route for preparing complex-shaped nanostructured materials as heterostructures [26,27].

The obtainment of heterostructures by the building blocks technique is yet a challenge. The possibility of homoaggregations shall be considered and minimized since it would have a deleterious outcome on the photocatalytic activity of the material. The formation of homoaggregations reduces the available surface area for the photocatalytic process and creates recombination sites for the photogenerated charges on the interface of the aggregated particles.

To maximize the formation of heteroaggregations, a fine control of the synthesis parameters is required, i.e., the proportion of reactants and the reaction time [6,24]. Previous works proposed kinetic models to describe the building blocks technique process and the influence of the synthesis parameters in the homo and heteroaggregations balance [6, 27]. The models were based on spherical nanoparticle morphology, merely modifying the particle's radius. Therefore, the applicability of these models to systems with variable morphology reactants, such as BiVO<sub>4</sub>, is hindered.

In this context, we studied in this work the formation of TiO<sub>2</sub>/BiVO<sub>4</sub> heterostructures based on heteroaggregation of preformed nanocrystals under hydrothermal conditions. The photocatalytic efficiency of the

heterostructured materials was used to evaluate the applicability of the synthesis method by comparing them with pristine anatase TiO<sub>2</sub> and *m*-BiVO<sub>4</sub>. The influencing factors were the molar ratio of the precursors, reaction time, and pH synthesis conditions.

## 2. Experimental section

### 2.1. Synthesis

Titanium dioxide was synthesized according to Mendonça and collaborators [28], where 5 mL of C<sub>12</sub>H<sub>28</sub>O<sub>4</sub>Ti (97%, Sigma Aldrich) was added in a 2:1 M ratio solution of H<sub>2</sub>O<sub>2</sub> (30%, Dinâmica) and NH<sub>4</sub>OH (28%, VETEC) respectively. The resulting solution, denominated peroxy ammonium titanate (PAT), was repeatedly heated to 60 °C and cooled in an ice bath until attaining a gel consistency. The yellow gel was washed with distilled water, centrifugated, dried at 80 °C, and macerated. The resulting powder was crystallized in distilled water with a concentration of 2 g L<sup>-1</sup> for 2 h at 200 °C in a hydrothermal reactor.

The BiVO<sub>4</sub> was prepared as described by Lopes and collaborators [29]. Firstly, 2.03 g of Bi(NO<sub>3</sub>)<sub>3</sub>•5H<sub>2</sub>O (98%, Éxodo Científica), 0.47 g of NH<sub>4</sub>VO<sub>3</sub> (99%, VETEC), and 2.5 mL of H<sub>2</sub>O<sub>2</sub> (30%, Dinâmica) were added to 117.5 mL of distilled water under vigorous stirring. The complex was crystallized at below 200 °C for 12 h in a hydrothermal reactor, and the result was the formation of a yellow powder, which was washed several times with distilled water and dried at 80 °C.

The heterostructures were assembled by the building blocks technique [6,24], using the TiO<sub>2</sub> (anatase) and the BiVO<sub>4</sub> (monoclinic) precursors described above. The synthesized precursors were added to an aqueous dispersion in different molar ratios (1:2, 1:1, 2:1, and 10:1 (TiO<sub>2</sub>:BiVO<sub>4</sub>)) in a hydrothermal reactor and crystallized under 200 °C for 12 h. The low solubility of the precursors in water maintains the ratio of the reagents added to the hydrothermal reactor after the synthesis reaction. During the pH tests, HNO<sub>3</sub> and KOH solutions adjusted the pH value inside the hydrothermal reactor to 4, 7, or 10.

For the precursor addition (PA) technique [23], a previously synthesized precursor was incorporated during the first stage of the second precursor synthesis process. The anatase TiO<sub>2</sub> was merged in the BiVO<sub>4</sub> synthesis process, producing the labeled TiO<sub>2</sub>/BiVO<sub>4</sub> PA sample, and the synthesized BiVO<sub>4</sub> was added during the PAT synthesis process, assembling the BiVO<sub>4</sub>:PAT PA sample. The molar ratio of the materials was kept at 2:1 of TiO<sub>2</sub>/BiVO<sub>4</sub>.

### 2.2. Characterization

X-ray diffraction (XRD), scanning electron microscopy (SEM), transmission electron microscopy (TEM), energy dispersive X-ray Spectroscopy (EDS), Fourier transform infrared spectroscopy (FTIR), ultraviolet–visible diffuse reflectance spectroscopy (DRS), Photoluminescence (PL), and time-resolved photoluminescence (TRPL) measurements were used to characterize the samples. N<sub>2</sub> adsorption at low temperature was used to obtain specific surface area (SSA) data applying the BET model. The measurement parameters and equipment

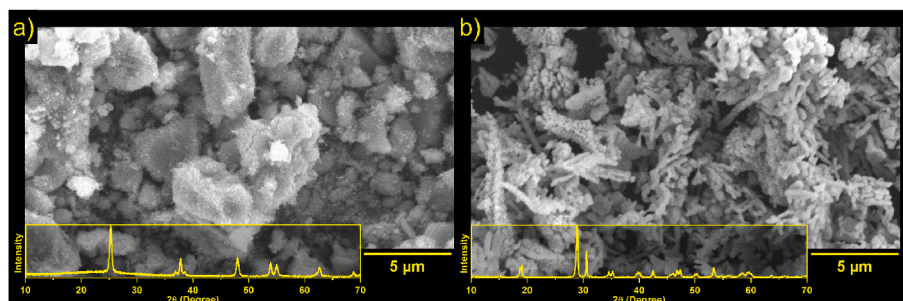


Fig. 1. SEM images and XRD spectrum of the: a) anatase TiO<sub>2</sub> and b) *m*-BiVO<sub>4</sub> precursors.

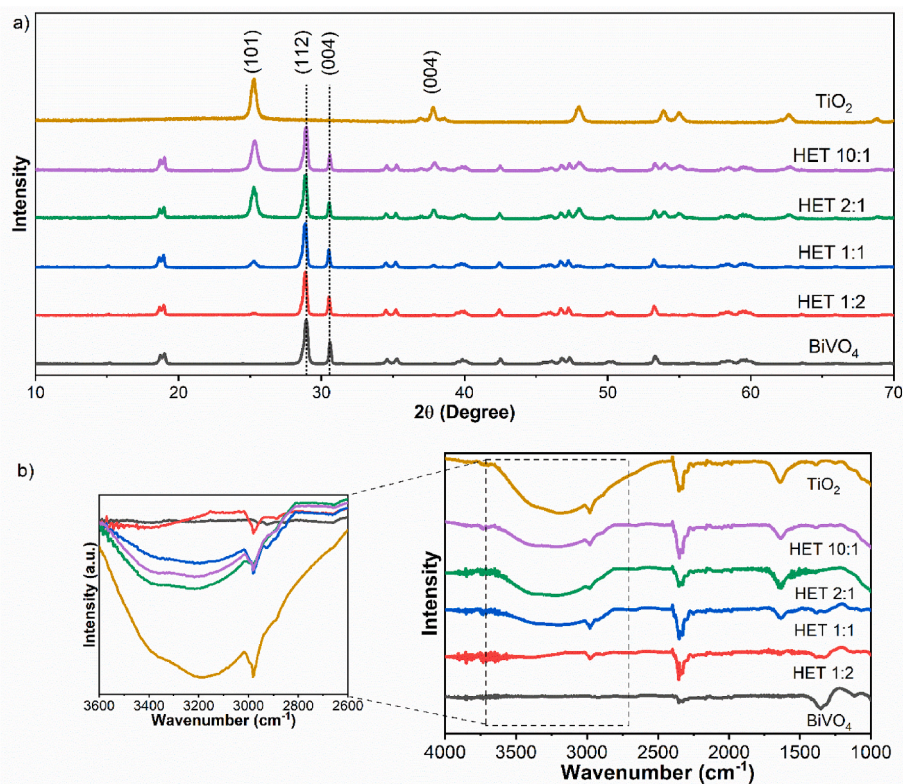


Fig. 2. XRD pattern (a) and FTIR spectra (b) of the building blocks heterostructures in 1:2, 1:1, 2:1, and 10:1 TiO<sub>2</sub>/BiVO<sub>4</sub> proportions and the neat precursors.

Table 1

Crystallite size calculated through Scherrer's equation.

Directions	TiO <sub>2</sub> 2 h	TiO <sub>2</sub> 12 h	<i>m</i> -BiVO <sub>4</sub>	1:2	1:1	2:1	10:1
[101] TiO <sub>2</sub>	17.0	19.4	–	20.9	18.6	18.1	17.4
[112] BiVO <sub>4</sub>	–	–	26.2	29.4	28.4	28.4	29.4

descriptions are presented in the supplementary information.

### 2.3. Photocatalytic properties

The photocatalytic properties of the heterostructures and precursors were investigated by analyzing the methylene blue (MB) degradation under visible (sunlight) and UV light ( $\lambda = 256$  nm) irradiation. For the experiments, 5 mg of the catalysts were taken into 20 mL of aqueous MB solution (5 mg L<sup>-1</sup>) and irradiated for 5 h. UV-Vis spectroscopy measures at 664 nm wavelength followed the MB concentration decay.

For the repeatability tests, the Het 2:1 annealed per 12 h was used for MB dye photodegradation under UV radiation. After the photocatalysis tests, the catalysts were washed and maintained immersed in distilled water for dye desorption. The procedure was performed in triplicate.

The photodegradation mechanism was evaluated by adding scavengers, potassium iodide (KI), and *tert*-butanol (TBA - C<sub>4</sub>H<sub>9</sub>OH), which were used to probe positive holes ( $h^+$ ) on semiconductors valence band and  $\bullet$ OH radical, respectively.

## 3. Results and discussions

The morphology and crystalline phase of the anatase TiO<sub>2</sub> and *m*-BiVO<sub>4</sub> precursors in Fig. 1 show that the TiO<sub>2</sub> precursor (Fig. 1(a)) exhibits agglomerates with different sizes and shapes [9,10,22]. At the same time, the BiVO<sub>4</sub> (Fig. 1(b)) reveals a fishbone-like morphology [30, 31]. The XRD patterns of the precursors inserted into the micrographs

exhibit well-defined diffraction peaks indexed according to the diffraction database PDF#21–1272 and PDF#75–1866 of anatase TiO<sub>2</sub> and monoclinic BiVO<sub>4</sub> (*m*-BiVO<sub>4</sub>), respectively.

The building block technique was used to tune the photocatalytic properties of TiO<sub>2</sub> and BiVO<sub>4</sub> with different (10:1, 2:1, 1:1, and 1:2) molar ratios by forming heterojunctions. The prepared heterostructures were analyzed by XRD and FTIR can be seen in Fig. 2. XRD patterns of the heterostructures in Fig. 2(a) show anatase TiO<sub>2</sub> and *m*-BiVO<sub>4</sub> phases. The intensity of the anatase TiO<sub>2</sub> diffraction peaks was directly dependent on the proportions.

Fig. 2(b) reveals stretching vibrations assigned to O–H groups at 3260 cm<sup>-1</sup>, whose intensity tends to increase at high TiO<sub>2</sub> ratios. Similar behavior is observed in the 1648 cm<sup>-1</sup> band, which is associated with bending modes of water Ti–OH [32]. A Bi–O bending vibration band can be noticed at 1356 cm<sup>-1</sup> [13]. In addition, a small band is observed at 2980 cm<sup>-1</sup>, associated with the C–H stretching of the titanium(IV) isopropoxide used in the PAT synthesis step [33].

The average crystallite size of the studied materials was calculated by Scherrer's equation [8,34] and arranged in Table 1. The results showed similar crystallite sizes for precursors and heterostructures, revealing unchanged crystal sizes after the formation of the heterostructures by the building blocks methodology.

Representative SEM images of the TiO<sub>2</sub>/BiVO<sub>4</sub> heterostructures are presented in Fig. 3(a–d), where the arrows point out TiO<sub>2</sub> regions. It is possible to observe several areas composed of both precursor materials. The morphology of the heterostructures was similar to the precursor SEM images in Fig. 1, as expected from the building blocks methodology [6,24]. It is an important feature of the system since it is ensured that heterostructures will keep the nanoparticles morphologies.

HRTEM image of the HET 10:1 sample in Fig. 3(e) evidence contact regions between TiO<sub>2</sub> and BiVO<sub>4</sub>. The image shows the lattice fringes corresponding to the interplanar distance of 0.348 nm to the (101) crystalline plane of TiO<sub>2</sub> and 0.312 nm associated with the (112) crystalline plane of BiVO<sub>4</sub>. The (400) crystalline plane was observed in both

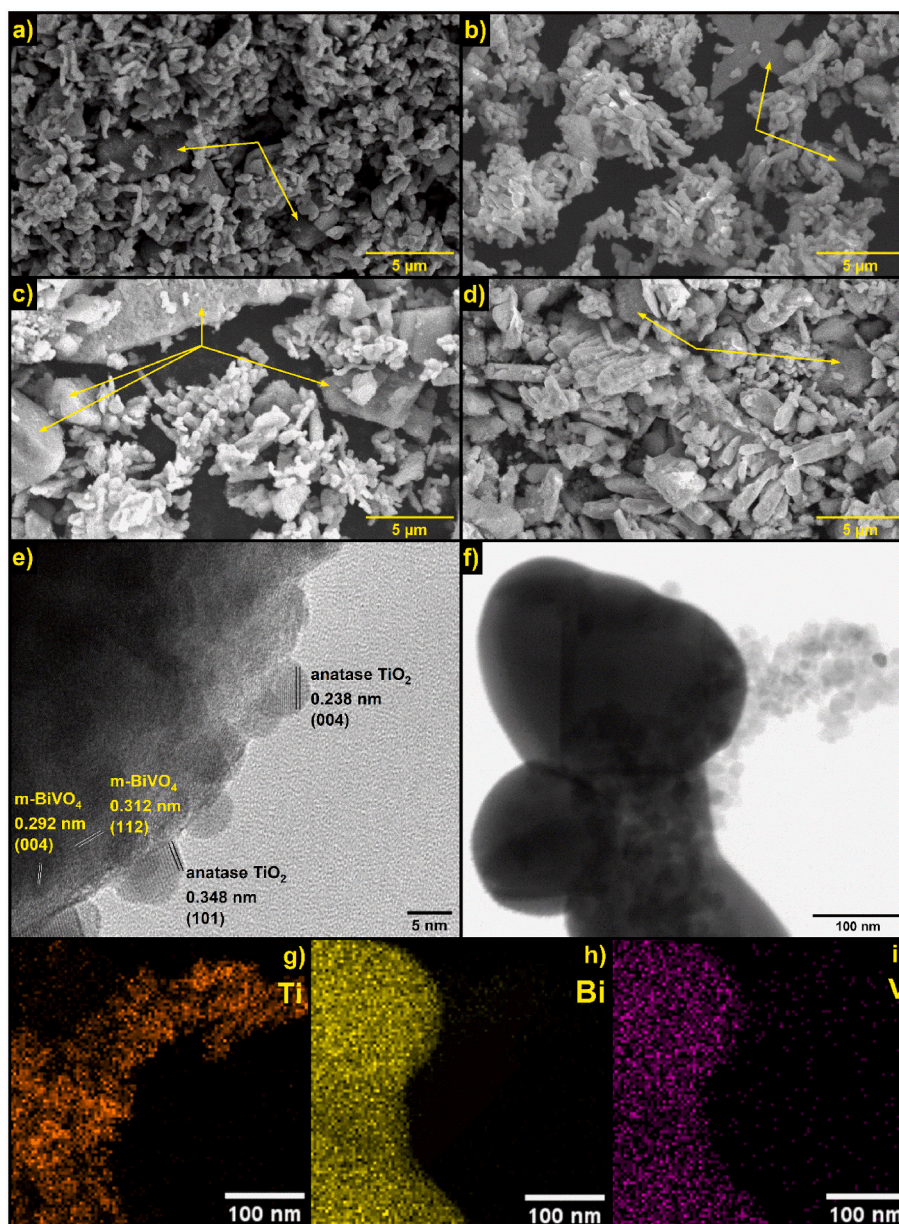


Fig. 3. SEM images of the a) Het 1:2, b) Het 1:1, c) Het 2:1, and d) Het 10:1 samples with the anatase  $\text{TiO}_2$  indicated; e) TEM image indicating the fringes and the interplanar distances in HET 10:1; f) HRTEM at the semiconductors contact area; EDX elemental mapping of g) Ti, h) Bi, and i) V.

$\text{TiO}_2$  and  $\text{BiVO}_4$  phases with interplanar distances of 0.238 nm and 0.292 nm, respectively. As proposed by Ribeiro et al., particle coalescence occurs with the collision or relative rotation of similarly orientated particles, called oriented attachment (OA) [27,35]. Thus, this is the primary mechanism for heterostructure formation under hydrothermal annealing.

The TEM image (Fig. 3(f)) and EDX mapping (Fig. 3(g–i)) show the materials interface region and the elemental distribution, respectively. The EDX measures confirm the occurrence of Ti, Bi, and V elements in distinct locations of the image. The image shows that the Bi and V elements are darker and more present in the structure and are covered with smaller  $\text{TiO}_2$  particles. Quantitative EDX analysis can be seen in Fig. S1.

The optical properties of the samples were studied using UV–vis diffuse reflectance spectroscopy (DRS), and the bandgap energy was experimentally determined by the Tauc plot from the line intersection in Fig. 4. The bandgap values for all the studied heterostructures are described in Table 2. The calculations were conducted assuming that *m*- $\text{BiVO}_4$  and anatase  $\text{TiO}_2$  have an indirect transition. As a result, the

bandgap of the  $\text{TiO}_2$  and  $\text{BiVO}_4$  precursors was given in 3.50 and 2.64 eV, respectively, corroborating with the bandgap values of the heterostructures in Table 2. Het 2:1 sample attained the values of 3.53 and 2.71 eV.

The specific surface area (SSA) and particle size of the heterostructures and precursors are shown in Table 3. The calculations and approximations used can be found in the supplementary material. Comparing the crystallite size information from Table 1 and the calculated diameter of the particles in Table 3, it is possible to consider that  $\text{TiO}_2$  is a monocrystalline material [36].

The photocatalytic activity of the synthesized heterostructures indicates the charge migration in the materials interface created by the heteroaggregation process during hydrothermal treatment. Therefore, photocatalytic activity can be used to evaluate the formation rate of heterostructures according to the synthesis parameters. The following set of equations describes the possibilities of particle interaction occurring during hydrothermal treatment and allows an understanding of the influence of the synthesis parameters on the heterostructures

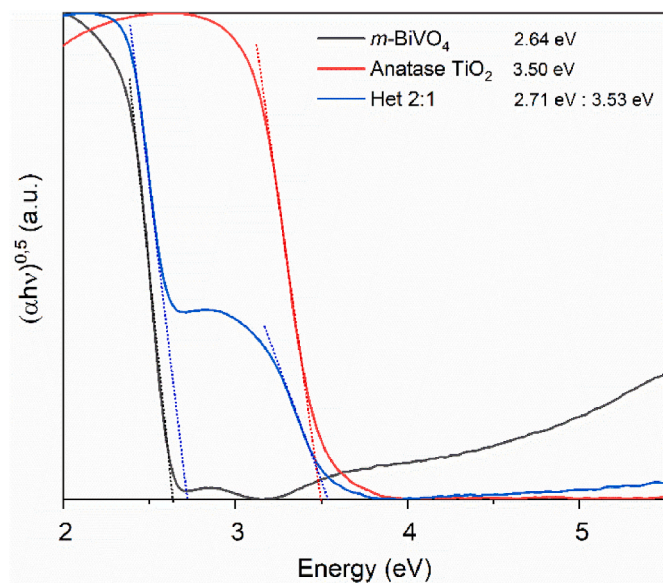


Fig. 4. UV-Vis DRS of m-BiVO<sub>4</sub>, anatase TiO<sub>2</sub>, and Het 2:1.

Table 2

Bandgap values of the samples Het 1:2, 1:1, 2:1, and 10:1.

Samples	Energy (eV) - Vis	Energy (eV) - UV
Het 1:2	2.61	3.41
Het 1:1	2.64	3.50
Het 2:1	2.71	3.53
Het 10:1	2.78	3.53

Table 3

Specific surface area of isolated samples and heterostructures.

Sample	SSA (m <sup>2</sup> g <sup>-1</sup> )	Apparent diameter (nm)
TiO <sub>2</sub> 2 h	69.7	20.3
TiO <sub>2</sub> 12 h	59.8	23.7
BiVO <sub>4</sub>	1.7	576
Het 1:2	13.7	-
Het 1:1	26.7	-
Het 2:1	45.6	-
Het 10:1	49.7	-

formation.

As mentioned, the reaction occurring in the building blocks technique produces homo- and heterostructures following the reactions below:



where equation (1) describes the heterostructure formation, while equations (2) and (3) describe homostructure formation. For the heterostructure formation, the rate law can be ascribed as:

$$\frac{d[(\text{TiO}_2/\text{BiVO}_4)_{\text{Heterostructure}}]}{dt} = k \cdot [\text{TiO}_2][\text{BiVO}_4] \quad 4$$

However, the quantitative value for [TiO<sub>2</sub>] and [BiVO<sub>4</sub>] is not simply their molar concentration since only the materials' surface is available to produce heterostructures. By analyzing equation (4), it is possible to infer that the increase in the species concentration results in enhancements in the rate of heterostructures formation. On the other hand, it is inaccurate since the rise in the species concentration raises the

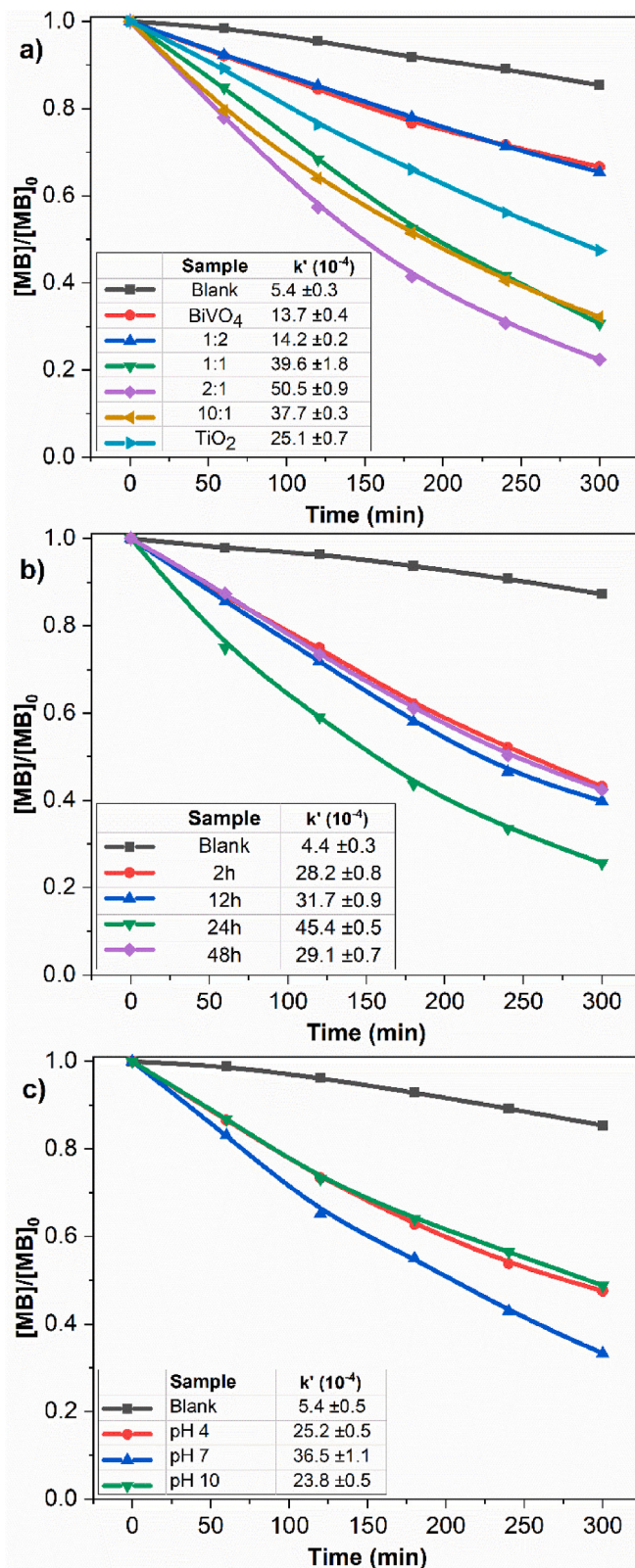


Fig. 5. Photodegradation of the MB dye under UV light irradiation in the presence of samples synthesized in different conditions: a) precursors molar ratio, b) treatment time, and c) pH.

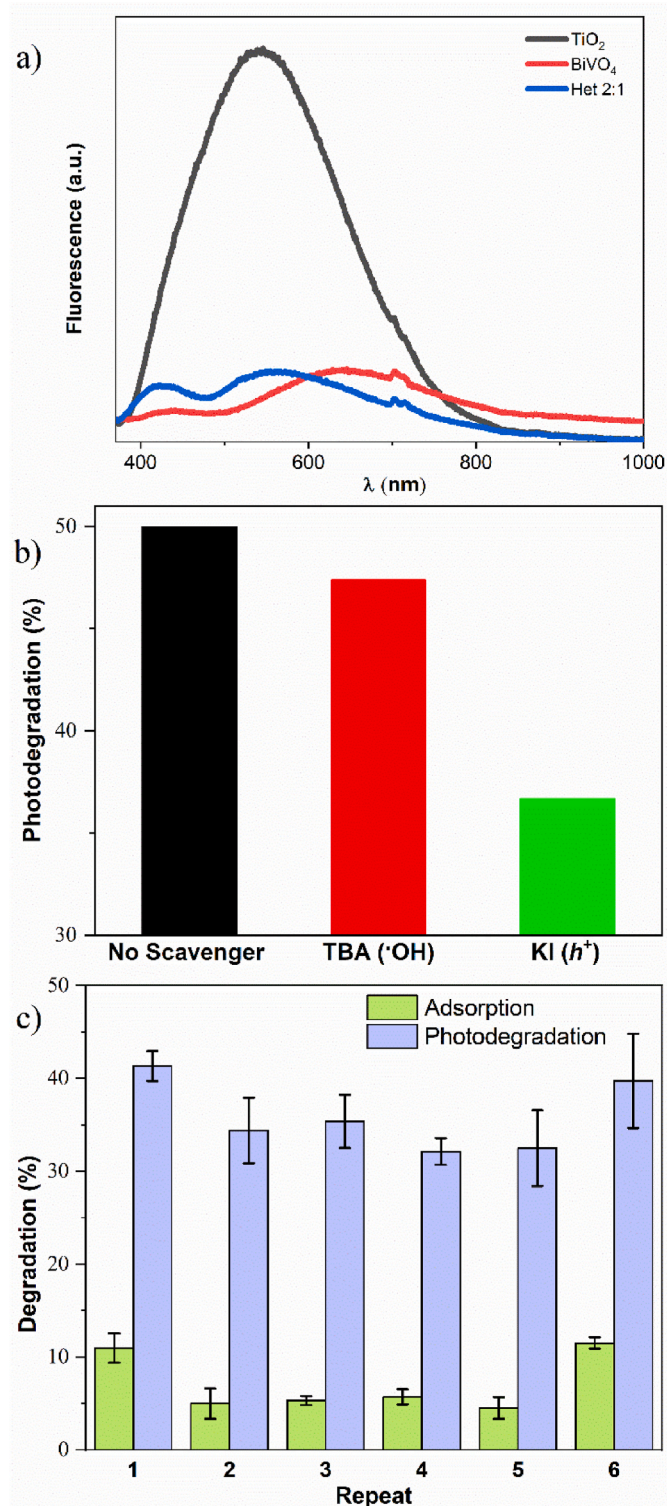


Fig. 6. Photoluminescence measurement of Het 2:1 and bare  $\text{TiO}_2$  and  $\text{BiVO}_4$  (a), MB dye photodegradation percentage catalyzed by the 2:1 sample with different scavengers during 3 h of UV light irradiation (b), and repeatability test in UV light irradiation (c).

possibility of homoaggregations formation, as described in equations (2) and (3). This fact can be directly seen in the TEM image shown in Fig. 3 (f). The homostructures have their particle movement in the medium surpassed because of their high hydrodynamic radius, and the capability of heterostructure formation can be reduced. Therefore, the fine control of the proportion of the material is a primordial factor for obtaining an

improved number of heterojunctions.

Fig. 5 displays the photocatalytic performance of the as-synthesized materials. Fig. 5(a) shows that the 2:1 ratio has better photocatalytic performance than the other ratios evaluated, demonstrating that this ratio achieves an adequate number of effective heterojunctions during hydrothermal treatment. The sample obtained with a ratio of 1:2 showed a photoactivity equivalent to the intact  $\text{BiVO}_4$  catalyst.

On the other hand, samples prepared with molar proportions varying from 1:1 to 10:1 showed superior photoactivity compared to the isolated  $\text{TiO}_2$  and  $\text{BiVO}_4$  catalysts. It is interesting to notice that the Het 2:1 sample, compared with Het 10:1, has a lower concentration of  $\text{TiO}_2$ , which is the most photoactive precursor. This fact evidences the importance of interface formation and the charge migration on the efficiency of the materials. It is essential to notice that the isolated  $\text{TiO}_2$  and  $\text{BiVO}_4$  materials, synthesized in the same conditions as the heterostructures, were also evaluated to exclude surface modifications. These tests aim to strengthen the hypothesis of the necessary charge migration, granting a contrast for the improved photoactivity of the heterostructures, which might be attributed to the charge migration through the interfaces between  $\text{TiO}_2$  and  $\text{BiVO}_4$  materials, shown by TEM images in Fig. 3.

Treatment time is also crucial for controlling the production of more active materials. From Fig. 5(b), we can observe that long reaction times alter the photocatalytic performance of the prepared materials. Heat treatment of the preformed materials in a 2:1 (Ti:Bi) ratio up to 24 h of reaction indicates significant improvement of the photocatalytic activity, possibly attributed to the formation of heterojunctions between the materials. However, the sample treated at 48 h decreased photocatalytic performance. This drop in behavior can be attributed to the formation of homojunctions that reduced the recombination of the electron-pair charge carriers less effectively than heterojunctions.

Finally, the heteroaggregation process can also be maximized by the electrostatic interaction of the particles. For this reason, the influence of the medium pH on the heterostructures formation was evaluated by synthesizing the Het 2:1 sample in different pH values. In the literature, the pH of the precursors  $\text{TiO}_2$  and  $\text{BiVO}_4$  are about 6 [37,38] and 3.5 [39–41], respectively. Fig. 5(c) shows no significant change in the photocatalytic properties of the heterostructure prepared at different pH, indicating that under the temperature conditions analyzed, pH has a negligible influence on the interaction between the particles.

Photoluminescence measurements were conducted to study the electron transportation in the Het 2:1 heterostructure and pristine  $\text{TiO}_2$  and  $\text{BiVO}_4$ . Fig. 6(a) demonstrates that  $\text{TiO}_2$  shows high-intensity emission excited at 355 nm, compared to  $\text{BiVO}_4$  and the evaluated heterostructure (Het 2:1), which showed similar intensities. This observed intensity is commonly associated with recombination rate, i.e., the  $\text{TiO}_2$  sample exhibits a higher recombination rate under UV radiation than pure  $\text{BiVO}_4$  and the heterostructure (Het 2:1) [42,43].

The primary reaction mechanism involved in the photodegradation process of the Het 2:1 catalyst was investigated utilizing scavengers of the reactive species. *Tert*-butyl alcohol (TBA) and iodide anions were used as trapping agents for hydroxyl radicals and photogenerated holes, respectively. The results in Fig. 6(b) show that there is no significant change in the photocatalytic ability of the tested materials in the presence of TBA, indicating that the indirect reaction mechanism, which involves hydroxyl radicals, has an unimportant involvement in the system. Conversely, the addition of iodide anions reduced the photodegradation capability of the Het 2:1 catalyst by approximately 30%, revealing that photogenerated holes play a critical role in the direct oxidation of the studied organic dye.

The repeatability test, in Fig. 6(c), was performed to observe Het 2:1 capability to maintain its photocatalytic response. The experiments were performed sequentially per 5 days, and the 6th measure was performed after 67 days of the first measure. The results reveal that the catalyst activity declined around 5% after the first measure, and the values kept stable during the sequential tests. Past 67 days from the first measure,

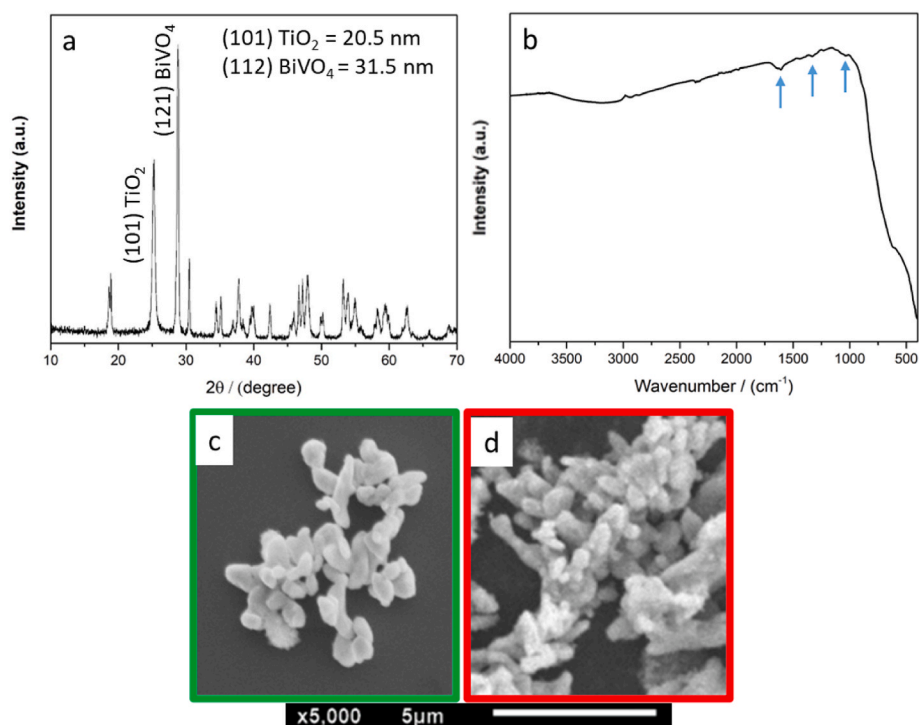


**Fig. 7.** Analyses of sample 2:1 after a photocatalytic cycle of 5 h, where a) is the XRD data, showing the crystallite sizes obtained by Scherrer equation; b) is the FTIR spectrum, indicating bands associated with MB presence; c) SEM images; d) SEM image of the catalyst previously to the photodegradation test.

Het 2:1 demonstrated MB photodegradation percentual comparable with its first use.

Maintaining the catalytic capacity of material even when stored and reused several times is an essential characteristic for scale-up processes. Therefore, the structural and morphological changes after photocatalytic tests were performed. Fig. 7 (a) shows the XRD data and the crystallite size obtained by the Scherrer equation. It is possible to observe that after 5 h active during the photodegradation test, the crystallite size has slightly altered, yet, the catalyst does not present structural modifications if compared with XRD data in Fig. 2 (a). Fig. 7 (b) exhibits the FTIR spectrum of the surface of the post-measurement catalyst, where low-intensity bands associated with MB presence confirm interactions of the catalyst with the MB dye [44]. This factor can be related to the slight drop in the catalyst capability to photodegradation after its first use. However, the presence of MB on its surface does not affect the catalyst's performance after the second cycle. After days of storage in distilled water, the MB might be desorbed from the catalyst surface or degraded, resulting in the recovery of the photodegradation capability of the catalyst as close as observed in its first use. The morphologies of the prepared materials were analyzed before (Fig. 7 (d)) and after (Fig. 7(c)) the photocatalytic tests and revealed no significant changes, indicating that the catalytic process occurs without catalyst dissolution. Therefore, the occurrence of a heterogeneous process is assured, which makes possible the reuse of the catalyst, as verified by the experimental data.

Despite intensive research, the main restrictions in heterogeneous photocatalysis remain related to the low utilization of visible light since most semiconductors need UV light to be activated [44]. Therefore, whereas the  $\text{BiVO}_4$  can be activated under visible radiation, experiments of MB dye photodegradation were carried out under solar light by samples annealed for 12, 24, and 48 h. The results, presented in Fig. 8 (a), demonstrated that the Het 2:1 annealed per 24 h reached increased photodegradation activity, surpassing bare  $\text{TiO}_2$ .

The heterojunction formation was evaluated from the lifetime ( $\tau$ ) of the charge carriers measured via time-resolved photoluminescence (TRPL) of the  $\text{BiVO}_4$  and 2:1 samples under visible radiation. Fig. 8(b)

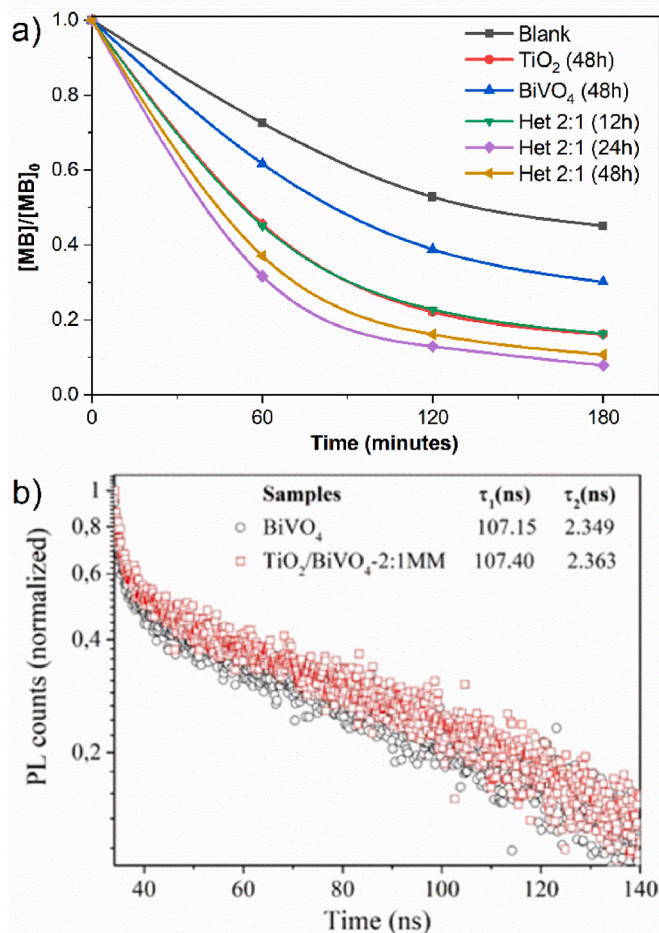


**Fig. 8.** Photodegradation test under visible light (a); and TRPL (lifetime decay) curves of the  $\text{BiVO}_4$  and 2:1 samples (b), where the powder was excited at 409 nm and photoluminescence was monitored at 545 nm.

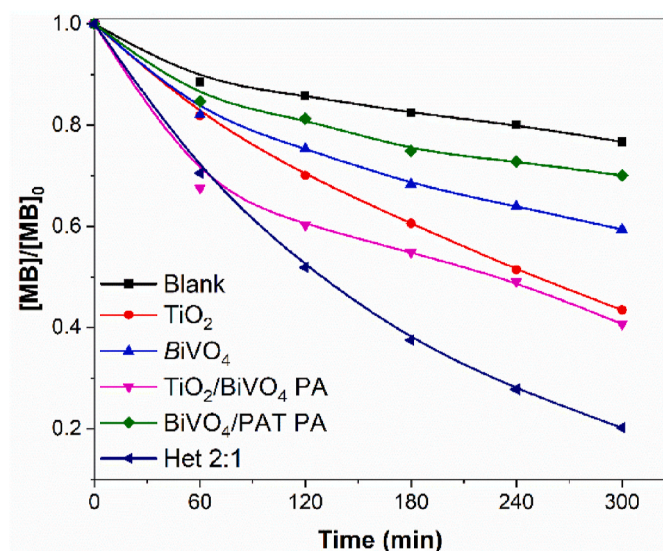


Fig. 9. Photocatalytic activity of prepared samples by building blocks and precursor addition methods.

exhibits the decay of PL intensity monitored at 545 nm and excited by a laser source centered at 409 nm for both samples. The PL decays of the samples were fitted with a first-order exponential function to calculate the lifetime of the electron/hole pair. The PL lifetime of the band-band emission (i.e., the electron/hole pair recombination) for the 2:1 sample was 107.40 ns. In comparison, the  $\text{BiVO}_4$  sample was approximately 107.15 ns, confirming the higher lifetime of the electron/hole pair of the heterostructure. This result agrees with the photoluminescence measurements in Fig. 6(a), ensuring that the heteroaggregation process successfully formed the heterojunction between  $\text{TiO}_2$  and  $\text{BiVO}_4$  during hydrothermal annealing of the preformed nanoparticles.

In Fig. 9, we can observe that Het 2:1 sample, prepared by the studied building blocks technique, had its photocatalytic activity compared with the heterostructures assembled by the precursor addition (PA) method.

The PA samples were prepared by adding  $\text{TiO}_2$  during the  $\text{BiVO}_4$  synthesis ( $\text{TiO}_2/\text{BiVO}_4$  PA) and  $\text{BiVO}_4$  during the PAT synthesis ( $\text{BiVO}_4/\text{PAT}$  PA). It is interesting to observe that the addition of another precursor during the  $\text{TiO}_2$  or the  $\text{BiVO}_4$  synthesis did not result in relevant variations in the MB photodegradation. This fact suggests that crystal growth based on heterogeneous nucleation is not an efficient mechanism for forming  $\text{TiO}_2/\text{BiVO}_4$  heterostructures. In contrast, improvements were found with the Het 2:1 sample from the building blocks technique, which was prepared with the improved synthesis conditions studied in this article.

In general, adjusting the synthesis parameters in the building blocks technique allowed reasonable control of the synthesis product. As illustrated in the compiled data of Fig. 10 (a), the kinetic of the collision of the particles in the hydrothermal reactor, which is guided by the proportion of precursors, medium pH, and time of treatment, favored the formation of heterojunctions over homojunctions. The generated heterostructures presented enhanced photoactivity under UV and sunlight radiation exposure compared with the pristine precursors. As mentioned, the photoactivity improvements might be attributed to the charges migration promoted by the formation of interfaces in the Het 2:1 heterostructure, as schematized in Fig. 10(b).

#### 4. Conclusions

The heteroaggregation of preformed materials from hydrothermal treatment was successfully explored in synthesizing  $\text{TiO}_2/\text{BiVO}_4$  heterostructured. The synthesis parameters such as materials proportion, treatment time, and pH influence the heterostructures formation. The micrographs confirm the intimate contact of the anatase  $\text{TiO}_2$  and  $m\text{-BiVO}_4$  particles in forming the desirable heterojunction. Besides, the photocatalytic performance of the synthesized materials in methylene blue photodegradation under UV radiation reveals that, except for Het 1:2, all the prepared heterostructures had enhanced photoactivity compared to pristine anatase  $\text{TiO}_2$  or  $m\text{-BiVO}_4$ . The higher activity was observed by the 2:1 proportion of  $\text{TiO}_2/\text{BiVO}_4$  annealed per 24 h in pH 7, which is attributed to the higher collision rate between the different materials during hydrothermal annealing. The photoactivity was also evaluated under visible light resulting in increased response compared

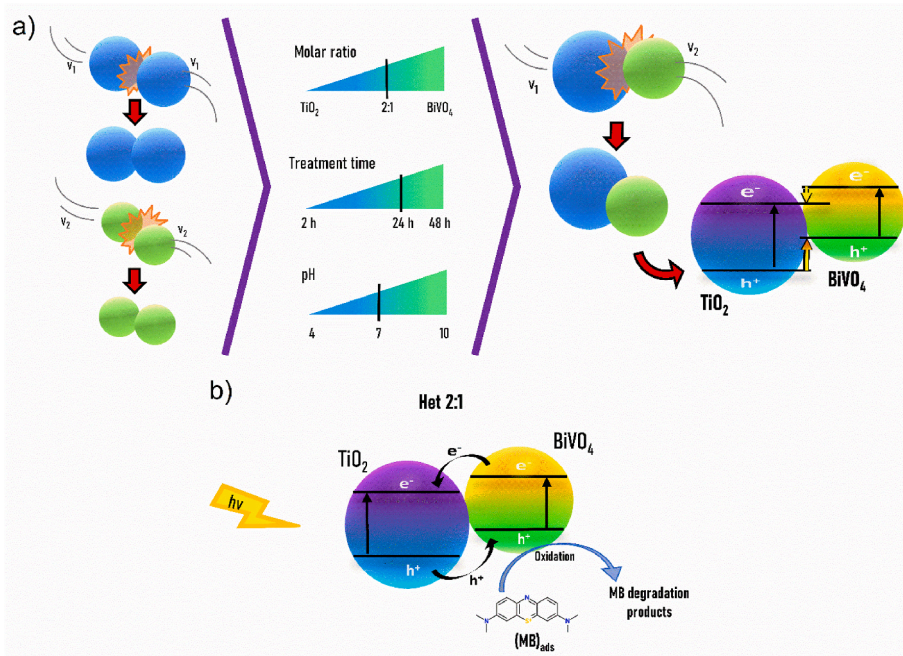


Fig. 10. Compiled data illustrating the influencing factors to promote heterojunctions of  $\text{TiO}_2$  and  $\text{BiVO}_4$  with higher photoactivity (a) and illustration of the charge migration occurring during the photodegradation of MB dye in the presence of Het 2:1 catalyst (b).

with anatase TiO<sub>2</sub> and *m*-BiVO<sub>4</sub> precursors. Repeatability tests show a photocatalytic efficiency decay of around 5% during sequential tests. A new measure with the same catalysts used for repeatability tests demonstrates that after 67 days, the catalysts are still operational. Additionally, the heterostructures prepared by the building blocks technique were verified to have improved photodegradation performance toward those prepared through the precursor addition technique, showing the proposed method's applicability in obtaining heterostructures composed of singly synthesized materials.

### CRedit authorship contribution statement

**Fernando C. Soares:** Conceptualization, Methodology, Validation, Formal analysis, Investigation, Writing – original draft. **Jéssica C. de Almeida:** Conceptualization, Methodology, Validation, Formal analysis, Investigation, Writing – review & editing. **Rafaella H. Koga:** Formal analysis, Investigation. **Douglas M. da Silva Del Duque:** Formal analysis, Investigation. **Gelson T.S.T. da Silva:** Formal analysis, Investigation, Writing – review & editing. **Caue Ribeiro:** Writing – review & editing, Funding acquisition. **Vagner R. de Mendonça:** Writing – review & editing, Supervision, Project administration, Funding acquisition.

### Declaration of competing interest

The authors declare that they have no known competing financial interests or personal relationships that could have appeared to influence the work reported in this paper.

### Data availability

Data will be made available on request.

### Acknowledgments

This study was partly financed by the Coordination for the Improvement of Higher Education Personnel - Brazil (CAPES)- Finance Code 001. We also thank CAPES/DS, FAPESP (Sao Paulo Research Foundation, process n° 2018/01258-5), CNPq (Brazilian National Council for Scientific and Technological Development, process n° 442575/2019-0, 468956/2014-0, and 409904/2016-3), and FINEP (Financier of Studies and Projects, project 01.17.0021.00) for the financial support. The authors thank the Agronano Network (Embrapa Research Network), the Agroenergy Laboratory, and the National Nanotechnology Laboratory for Agribusiness (LNNA) for providing institutional support and facilities.

### Appendix A. Supplementary data

Supplementary data to this article can be found online at <https://doi.org/10.1016/j.matchemphys.2022.126588>.

### References

- [1] D.A. Giannakoudakis, When sonochemistry meets heterogeneous photocatalysis: designing a sonophotoreactor towards sustainable selective oxidation, *Green Chem.* (2020) 11.
- [2] Z. Zhang, M. Wang, W. Cui, H. Sui, Synthesis and characterization of a core-shell BiVO<sub>4</sub>@g-C<sub>3</sub>N<sub>4</sub> photo-catalyst with enhanced photocatalytic activity under visible light irradiation, *RSC Adv.* 7 (2017) 8167–8177.
- [3] G.T.S.T. da Silva, K.T.G. Carvalho, O.F. Lopes, C. Ribeiro, g-C<sub>3</sub>N<sub>4</sub>/Nb<sub>2</sub>O<sub>5</sub> heterostructures tailored by sonochemical synthesis: enhanced photocatalytic performance in oxidation of emerging pollutants driven by visible radiation, *Appl. Catal. B Environ.* 216 (2017) 70–79.
- [4] E. Gallegos, F. Muñoz Bisesti, K. Vaca-Escobar, C. Santacruz, L. Fernández, A. Debut, P.J. Espinoza-Montero, Degradation of direct blue 1 through heterogeneous photocatalysis with TiO<sub>2</sub> irradiated with E-beam, *Processes* 8 (2020) 1181.
- [5] E. Giamello, G. Pacchioni, Applied vs fundamental research in heterogeneous photocatalysis: problems and perspectives. An introduction to 'physical principles of photocatalysis', *J. Phys. Condens. Matter* 32 (2020), 360301.
- [6] V.R. de Mendonça, C.J. Dalmaschio, E.R. Leite, M. Niederberger, C. Ribeiro, Heterostructure formation from hydrothermal annealing of preformed nanocrystals, *J. Mater. Chem. A* 3 (2015) 2216–2225.
- [7] S.N. Ahmed, W. Haider, Heterogeneous photocatalysis and its potential applications in water and wastewater treatment: a review, *Nanotechnology* 29 (2018), 342001.
- [8] J.C. de Almeida, M.T. Corrêa, R.H. Koga, D.M.S. Del Duque, O.F. Lopes, G.T.S.T. da Silva, C. Ribeiro, V.R. de Mendonça, Crystallization time in ZnO: the role of surface OH groups in its photoactivity, *New J. Chem.* (2020) 18216–18224.
- [9] S. Challagulla, K. Tarafder, R. Ganesan, S. Roy, Structure sensitive photocatalytic reduction of nitroarenes over TiO<sub>2</sub>, *Sci. Rep.* 7 (2017) 8783.
- [10] V. Castrejón-Sánchez, R. López, M. Ramón-González, Á. Enriquez-Pérez, M. Camacho-López, G. Villa-Sánchez, Annealing control on the anatase/rutile ratio of nanostructured titanium dioxide obtained by sol-gel, *Crystals* 9 (2018) 22.
- [11] N. Jiang, Y. Du, P. Ji, S. Liu, B. He, J. Qu, J. Wang, X. Sun, Y. Liu, H. Li, Enhanced photocatalytic activity of novel TiO<sub>2</sub>/Ag/MoS<sub>2</sub>/Ag nanocomposites for water-treatment, *Ceram. Int.* 46 (2020) 4889–4896.
- [12] C.N.C. Hitam, A.A. Jalil, A review on exploration of Fe<sub>2</sub>O<sub>3</sub> photocatalyst towards degradation of dyes and organic contaminants, *J. Environ. Manag.* 258 (2020), 110050.
- [13] Y. Cheng, Y. Yang, Z. Jiang, L. Xu, C. Liu, Fabrication and characterization of a novel composite magnetic photocatalyst β-Bi<sub>2</sub>O<sub>3</sub>/BiVO<sub>4</sub>/Mn<sub>x</sub>Zn<sub>1-x</sub>Fe<sub>2</sub>O<sub>4</sub> for rhodamine B degradation under visible light, *Nanomaterials* 10 (2020) 797.
- [14] X. Meng, Z. Li, Z. Zhang, Pd-nanoparticle-decorated peanut-shaped BiVO<sub>4</sub> with improved visible light-driven photocatalytic activity comparable to that of TiO<sub>2</sub> under UV light, *J. Catal.* 356 (2017) 53–64.
- [15] S.J.A. Moniz, S.A. Shevlin, D.J. Martin, Z.-X. Guo, J. Tang, Visible-light driven heterojunction photocatalysts for water splitting – a critical review, *Energy Environ. Sci.* 8 (2015) 731–759.
- [16] J. Xu, Y. Wang, J. Niu, M. Chen, Facile construction of BiOBr/BiOOCOOH p-n heterojunction photocatalysts with improved visible-light-driven photocatalytic performance, *Separ. Purif. Technol.* 225 (2019) 24–32.
- [17] Z. Ma, X. Li, C. Zhou, L. Deng, G. Fan, TiO<sub>2</sub>/BiVO<sub>4</sub>, a heterojunctioned microfiber with enhanced photocatalytic performance for methylene blue under visible light irradiation, *Chin. J. Chem. Phys.* 30 (2017) 153–160.
- [18] C. Xia, H. Wang, J.K. Kim, J. Wang, Rational design of metal oxide-based heterostructure for efficient photocatalytic and photoelectrochemical systems, *Adv. Funct. Mater.* (2020), 2008247.
- [19] G. Qiu, T. Wang, X. Li, X. Tao, B. Li, Novel BiOCl/BiCl<sub>3</sub>Br-CTA heterostructure photocatalyst with abundant oxygen vacancies and a superoleophilic surface for promoting selective oxidation of toluene, *Ind. Eng. Chem. Res.* 59 (2020) 11517–11526.
- [20] Y. Shang, T. Wang, Y. Xiao, Z. Dong, X. Li, B. Li, Constructing BiOBr/CoOx/g-C<sub>3</sub>N<sub>4</sub> Z-scheme photocatalyst with CoOx as both redox mediator and cocatalyst for phenol degradation, *J. Alloys Compd.* 875 (2021), 159998.
- [21] H. Khan, M.G. Rigamonti, G.S. Patience, D.C. Boffito, Spray dried TiO<sub>2</sub>/WO<sub>3</sub> heterostructure for photocatalytic applications with residual activity in the dark, *Appl. Catal. B Environ.* 226 (2018) 311–323.
- [22] F. Khalid, M. Tabish, K.A.I. Bora, Novel poly(vinyl alcohol) nanofiltration membrane modified with dopamine coated anatase TiO<sub>2</sub> core shell nanoparticles, *J. Water Proc. Eng.* 37 (2020), 101486.
- [23] R.T. Bueno, O.F. Lopes, K.T.G. Carvalho, C. Ribeiro, H.A.J.L. Mourão, Heterostructured semiconductors: an approach about the main challenges for obtaining and application on environmental and energy photochemical processes, *Quim. Nova* 42 (2019) 661–675.
- [24] V.R. de Mendonça, W. Avansi, R. Arenal, C. Ribeiro, A building blocks strategy for preparing photocatalytically active anatase TiO<sub>2</sub>/rutile SnO<sub>2</sub> heterostructures by hydrothermal annealing, *J. Colloid Interface Sci.* 505 (2017) 454–459.
- [25] I.A. de Castro, W. Avansi, C. Ribeiro, WO<sub>3</sub>/TiO<sub>2</sub> heterostructures tailored by the oriented attachment mechanism: insights from their photocatalytic properties, *CrystEngComm* 16 (2014) 1514–1524.
- [26] K.-S. Cho, D.V. Talapin, W. Gaschler, C.B. Murray, Designing PbSe nanowires and nanorings through oriented attachment of nanoparticles, *J. Am. Chem. Soc.* 127 (2005) 7140–7147.
- [27] C. Ribeiro, E.J.H. Lee, E. Longo, E.R. Leite, A kinetic model to describe nanocrystal growth by the oriented attachment mechanism, *ChemPhysChem* 6 (2005) 690–696.
- [28] V.R. de Mendonça, O.F. Lopes, W. Avansi, R. Arenal, C. Ribeiro, Insights into formation of anatase TiO<sub>2</sub> nanoparticles from peroxo titanium complex degradation under microwave-assisted hydrothermal treatment, *Ceram. Int.* 45 (2019) 22998–23006.
- [29] O.F. Lopes, K.T.G. Carvalho, G.K. Macedo, V.R. de Mendonça, W. Avansi, C. Ribeiro, Synthesis of BiVO<sub>4</sub> via oxidant peroxo-method: insights into the photocatalytic performance and degradation mechanism of pollutants, *New J. Chem.* 39 (2015) 6231–6237.
- [30] X. Lin, H. Li, L. Yu, H. Zhao, Y. Yan, C. Liu, H. Zhai, Efficient removal rhodamine B over hydrothermally synthesized fishbone like BiVO<sub>4</sub>, *Mater. Res. Bull.* 48 (2013) 4424–4429.
- [31] T. Yu, L. Lv, H. Wang, X. Tan, Enhanced photocatalytic treatment of Cr(VI) and phenol by monoclinic BiVO<sub>4</sub> with {010}-orientation growth, *Mater. Res. Bull.* 107 (2018) 248–254.

- [32] A. León, P. Reuquen, C. Garín, R. Segura, P. Vargas, P. Zapata, P. Orihuela, FTIR and Raman characterization of TiO<sub>2</sub> nanoparticles coated with polyethylene glycol as carrier for 2-methoxyestradiol, *Appl. Sci.* 7 (2017) 49.
- [33] N. Hafizah, I. Sopyan, Nanosized TiO<sub>2</sub> photocatalyst powder via sol-gel method: effect of hydrolysis degree on powder properties, 2009, *Int. J. Photoenergy* (2009) 1–8.
- [34] M. Rakhra, N. Verma, S. Bhatia, Structural, morphological, optical, electrical and agricultural properties of solvent/ZnO nanoparticles in the photodegradation of DR-23 dye, *J. Electron. Mater.* 49 (2020) 643–649.
- [35] C. Ribeiro, E.J.H. Lee, T.R. Girdali, E. Longo, J.A. Varela, E.R. Leite, Study of synthesis variables in the nanocrystal growth behavior of tin oxide processed by controlled hydrolysis, *J. Phys. Chem. B* 108 (2004) 15612–15617.
- [36] V.R. de Mendonça, C. Ribeiro, Influence of TiO<sub>2</sub> morphological parameters in dye photodegradation: a comparative study in peroxy-based synthesis, *Appl. Catal. B Environ.* 105 (2011) 298–305.
- [37] E. Al-Hetlani, M.O. Amin, M. Madkour, Detachable photocatalysts of anatase TiO<sub>2</sub> nanoparticles: annulling surface charge for immediate photocatalyst separation, *Appl. Surf. Sci.* 411 (2017) 355–362.
- [38] M. Kaneko, Anatase TiO<sub>2</sub> adsorption on 3-aminopropyltrimethoxysilane-modified Al or glass surfaces, *Heliyon* 5 (2019), e01734, <https://doi.org/10.1016/j.heliyon.2019.e01734>.
- [39] M. Favaro, R. Uecker, S. Nappini, I. Pís, E. Magnano, H. Bluhm, R. van de Krol, D. E. Starr, Chemical, structural, and electronic characterization of the (010) surface of single crystalline bismuth vanadate, *J. Phys. Chem. C* 123 (2019) 8347–8359.
- [40] Y. Hermans, C. Olivier, H. Junge, A. Klein, W. Jaegermann, T. Toupance, Sunlight selective photodeposition of CoO<sub>x</sub>(OH)<sub>y</sub> and NiO<sub>x</sub>(OH)<sub>y</sub> on truncated bipyramidal BiVO<sub>4</sub> for highly efficient photocatalysis, *ACS Appl. Mater. Interfaces* 12 (2020) 53910–53920.
- [41] K. Pingmuang, J. Chen, W. Kangwansupamonkon, G.G. Wallace, S. Phanichphant, A. Nattestad, Composite photocatalysts containing BiVO<sub>4</sub> for degradation of cationic dyes, *Sci. Rep.* 7 (2017) 8929.
- [42] R. Wang, J. Bai, Y. Li, Q. Zeng, J. Li, B. Zhou, BiVO<sub>4</sub>/TiO<sub>2</sub>(N<sub>2</sub>) nanotubes heterojunction photoanode for highly efficient photoelectrocatalytic applications, *Nano-Micro Lett.* 9 (2017) 14.
- [43] S. Mansour, R. Akkari, S. Ben Chaabene, M. Saïd Zina, Effect of surface site defects on photocatalytic properties of BiVO<sub>4</sub>/TiO<sub>2</sub> heterojunction for enhanced methylene blue degradation, *Adv. Mater. Sci. Eng.* 2020 (2020), 6505301.
- [44] Y. Xiao, Z. He, R. Wang, X. Tao, B. Li, Synthesis of WO<sub>3</sub> nanofibers decorated with BiOCl nanosheets for photocatalytic degradation of organic pollutants under visible light, *Colloids Surf. A Physicochem. Eng. Asp.* 580 (2019), 123752.